LAWRENCE
LIVERMORE
NATIONAL
LABORATORY

LLNL-JRNL-825654

Shock tube investigation of high-temperature, extremely-rich oxidation of several Co-Optima biofuels for spark-ignition engines

R. Rahman, S. Barak, S. W. Wagnon, G. Kukkadapu, S. S. Vasu

August 10, 2021

Combustion and Flame

Disclaimer

Shock tube investigation of high-temperature, extremely-rich oxidation of several Co-Optima biofuels for spark-ignition engines

Ramees K. Rahman[a, b], Samuel Barak[a, b], Scott W. Wagnon[c], Goutham Kukkadapu[c], William J. Pitz[c], Subith S. Vasu[a,b,d]

[a]Mechanical and Aerospace Engineering, University of Central Florida, 4000 Central Florida Blvd., Orlando, FL 32816-2450, USA

[b]Center for Advanced Turbomachinery and Energy Research (CATER), University of Central Florida, 4000 Central Florida Blvd., Orlando, FL 32816-2450, USA

[c]Materials Science Division, Lawrence Livermore National Laboratory, 7000 East Avenue Livermore, CA 94551, USA

[d]CREOL, The College of Optics and Photonics, University of Central Florida, Orlando, FL 32816, USA

[*]Corresponding author: Prof. Subith Vasu, email: subith@ucf.edu, phone: +1-407-823-3468

Abstract

To reduce the reliance on fossil fuels in the transportation sector and increase combustion efficiency, the Co-Optima initiative from US Department of Energy identified the top 10 biofuels for downsized, boosted, spark-ignition engines. Most of these biofuels have detailed reaction mechanisms available in literature developed based on studies at temperatures lower than 1700 K and an equivalence ratio of less than five. As such, the performance of these detailed mechanisms at high temperature and extremely rich conditions are unknown. It is important to validate kinetic mechanisms at these conditions because they are conducive to soot formation. Prediction of soot by chemical kinetic models relies on the prediction of underlying benchmark species like carbon monoxide and ethylene. In this work, we conduct high temperature (1700-2050 K) and high equivalence ratio(Φ=8.6) oxidation of these biofuels, namely 2,4,4-trimethyl-1-pentene (α-diisobutylene), ethanol, cyclopentanone, methyl acetate, and 2-methylfuran, blended in ethylene behind reflected shock waves at 4-4.7 atm pressure. Carbon monoxide and ethylene time histories are measured simultaneously using a continuous feedback quantum cascade laser near 4.9 µm and a tunable CO_2 gas laser at 10.532 nm, respectively. Results show that ethanol blend forms more carbon monoxide than other biofuels and consumes ethylene faster than the biofuel blends in the

LLNL-JRNL-825654

temperature range considered. The performance of different mechanisms in literature are evaluated against the experimental results. The novel reaction mechanism 'the Co-Optima model', which includes the sub mechanisms for all the biofuels in this study, was found to be the best mechanism for the experimental conditions studied.

Keywords: biofuel, shock tube, species histories, reaction mechanism.

1. Introduction

The high volatility in crude oil price, excessive reliance on fossil fuels, and the environmental issues caused by burning fossil fuels have ignited the need for finding alternative solutions. One of the significant consumers of fossil fuels is the transportation sector. Reducing the consumption of fossil fuels in the transportation sector can be achieved by developing advanced engines with high combustion efficiency and by developing advanced, oxygenated biofuels that burn at high efficiency [1-5]. The United States Department of Energy started this initiative, known as Co-Optima, to develop advanced engines and fuels to enhance efficiency and reduce environmental impact[6]. Under the Co-Optima initiative, top ten fuels for spark-ignition engines were outlined based on rigorous screening criteria, including health hazard assessments, biodegradability, fuel properties, feasibility of synthesis, etc.[5, 7]. This includes 2,4,4-trimethyl 1-pentene (α-diisobutylene), ethanol, cyclopentanone, methyl acetate, and methylfuran, which are the five biofuels of interest in this work. They were chosen for this study based on the various functional groups represented and to probe fuel molecular influences on combustion.

There have been some studies of these compounds in the literature. Metcalfe et al.[8] studied the ignition delay times during the oxidation of 2,4,4 trimethyl 1-pentene (α-DIB), 2,4,4 trimethyl 2-pentene, and their blends at fuel-lean and stoichiometric conditions (ϕ=0.25-1) within the temperature range of 1200-1550 K at 1-4 atm. They found that the 2-pentene isomer ignites faster than the 1-pentene isomer, and the ignition delays of their blends were directly proportional to the fraction of each isomer present. They also developed a kinetic mechanism for predicting ignition delays and were able to capture these trends. Using this mechanism, they found that the ignition delay times of α-isomer to be more sensitive to the decomposition reaction of isobutene than to the decomposition of the fuel molecule itself. In contrast, the 2-pentene isomer decomposition proceeded through the formation of resonant stabilized radicals. Hu et al.[9] studied ignition delay of α-DIB behind reflected shockwaves at 2-10 atm pressure and temperature range of 1200-1650 K at an equivalence ratio of 0.5-2.0. They found that Metcalfe et al. model over-predicted ignition delay and optimized the model by altering reactions related to isobutene

and α-DIB as well as updating thermochemical data from the literature. The modified model improved the prediction of ignition delay against their experimental data. Later, Li et al.[10] conducted shock tube experiments to determine ignition delay of gasoline surrogate fuel containing di-isobutylene within the temperature range of 950-1300 K and pressure range of 10-20 bar at an equivalence ratio 0.5-2.0. They also developed a kinetic model which contains 563 species and 2915 reactions and was able to predict the ignition delay of this surrogate at high pressure satisfactorily. The literature studies were conducted at temperatures less than 1700 K and no data exist in literature for α-DIB beyond this temperature. Additionally, no experimental data is available for combustion at extremely rich conditions (Φ>5.0) for α-DIB.

Though most of the shock tube studies on ethanol focus on global kinetic parameters like ignition delay[11], few studies in the literature measures species/radical concentrations using techniques like atomic resonance absorption spectroscopy (ARAS)[12], laser absorption spectroscopy[13, 14] and time of flight mass spectrometry (TOF-MS)[15]. The methods like ARAS and laser absorption spectroscopy provide results with higher accuracy and very high time resolution as compared to TOF-MS. Using shock tube experiments and TOF-MS, Kiecherer et al.[16] determined the reaction rate of unimolecular decomposition of ethanol to ethylene and water but with high uncertainty of 40%. Pinzon et al.[17] conducted shock tube studies at 1.31 atm within the temperature range of 1250-1677 K and measured H_2O time-histories with laser absorption spectroscopy near 1388.139 nm. Since unimolecular decomposition of ethanol was the only contributor for water formation during the first few microseconds, the time-history obtained was used to determine the rate of the reaction C_2H_5OH (+M) = C_2H_4 + H_2O, narrowing down the uncertainty of this reaction to ±20%. Laich et al.[14] measured carbon monoxide time-histories behind reflected shock waves during oxidation of ethanol within the temperature range of 960-1580 K and pressure range of 17.8-23.9 atm at lean and stoichiometric conditions. They compared the results obtained with models from the literature and found that the models fail to predict CO time-histories, especially at lower temperatures (~1250 K). They also highlight the importance of secondary radical of ethanol in the formation of carbon monoxide using pathway and sensitivity analysis. From review of literature studies, it is clear that having more information on species formed during combustion helps in fine tuning the comparatively well studied kinetics of ethanol. Additionally, literature lacks experimental data at extremely rich oxidation of ethanol (Φ>5.0) for temperature greater than 1700 K and hence the validity of reaction mechanisms at these conditions are unknown.

Another oxygenated biofuel of interest in the Co-Optima initiative is cyclopentanone. The ignition delays of lean(Φ=0.5), stoichiometric and rich mixtures (Φ=2.0) of cyclopentanone were studied in shock tube by Zhang et al.[18] within the temperature range of 768-1368 K and pressure range of 15-30 bar using a shock tube and rapid compression machine (RCM). Understanding ignition delay characteristics is one of the first steps in improving our understanding of the kinetics of a new biofuel. They also measured carbon monoxide time-histories within a temperature range of 1100 K – 1300 K, which was used to validate a reaction mechanism. Their reaction mechanism was able to predict the trend in ignition delay and CO time-histories during cyclopentanone oxidation. Dong et al.[19] studied pyrolysis of cyclopentanone in a shock tube at a temperature range of 1156-1416 K and a pressure range of 8.5-10.0 atm. They used laser absorption spectroscopy to measure carbon monoxide and ethylene time-histories during cyclopentanone pyrolysis. They used a reaction mechanism generator to generate a model containing 821 species and 79589 reactions. Their model predicted CO mole fraction similar to Thion et al.[20] model but differed in the ratio of ethylene to carbon monoxide. They used the ratio of ethylene to carbon monoxide to show the importance of radical involved bimolecular pathways in cyclopentanone pyrolysis. These studies were at a temperature lower than 1700 K and an equivalence ratio less than 5.0. Hence the performance of these mechanisms at high temperatures and during extremely rich oxidation is unknown.

Methyl acetate is another oxygenated biofuel under the Co-Optima initiative, derived from vegetable oils and animal fats[21]. Farooq et al.[22] studied the pyrolysis of methyl esters at a temperature range of 1260-1653 K and a pressure range of 1.4-1.7 atm. They used laser absorption spectroscopy to measure carbon dioxide formed using a tunable diode laser at 2.7 μm. Their results indicated the existence of a direct pathway for the formation of CO_2 from esters rather than the rapid formation of two oxygenated radicals. Later, Ren et al.[23] conducted shock tube experiments for pyrolysis and stoichiometric oxidation of methyl acetate within the temperature range of 1400-1700 K and pressures around 1.5 atm. They measured species time-histories for CO, CO_2, OH, and H_2O using laser absorption spectroscopy. They determined a rate constant of the unimolecular decomposition reaction of methyl acetate ($CH_3COOCH_3=2CH_3+CO_2$) and its branching ratio, which agreed with experimental and theoretical studies in the literature. Ahmed et al.[24] determined ignition delay times during lean, stoichiometric, and rich oxidation of methyl acetate behind reflected shock waves within a temperature range of 1000-1450 K and a pressure range of 15-30 bar. They also conducted speciation studies in a jet stirred reactor within a temperature range of 800-1100 K at atmospheric pressure for methyl acetate at equivalence ratios 0.5 and 1.0. Using theoretical calculations, they determined the reaction rates for H-abstraction reactions. They presented a modified kinetic mechanism that could predict the experimental

ignition delay times and species profiles in a jet-stirred reactor (JSR) satisfactorily. However, the performance of these models beyond 1700 K and extremely rich conditions (Φ>5.0) are still unknown, and experimental data are required at these conditions to validate detailed kinetic models.

2-Methylfuran is a biofuel that can be derived from biomass sources using production methods through the synthesis of furfurals[25]. Somers et al.[26] studied the ignition delay times of 2-methylfuran in a shock tube within the temperature range of 1200-1800 K at atmospheric pressure and for equivalence ratios of 0.5-2.0. They also developed a detailed kinetic mechanism with 391 species and 2059 reactions, which could predict their experimental results at all equivalence ratios with reasonable accuracy. Their rate of production and sensitivity analyses revealed that hydrogen abstraction by H atom promoted reactivity and H atom addition to the furan ring inhibited reactivity. Ugyun et al.[27] conducted high pressure (40 bar) shock tube ignition delay measurements for 2-methylfuran within the temperature range of 820-1215 K at an equivalence ratio of 1.0. By sensitivity analysis using Somers et al.[28] mechanism, they confirmed that abstraction by H atom to be the important reaction at high temperature (~1400 K) while at intermediate temperature (~1200 K), H abstraction by OH radicals seems to be more critical. Later, Tran et al.[29] developed a reaction mechanism for furanic fuels using the speciation measurements in a JSR within the temperature range of 730-1170 K and at 1 bar. These measurements were made at a lower temperature (<1700 K), measured global kinetic parameters like ignition delay, and were at an equivalence ratio less than 5.0. Recently, Barak et al. [30] looked at the formation of soot during combustion of these fuels and found that ethanol produced the least soot under similar conditions compared to the other four fuels. Experimental data at high temperature (>1700 K) and extremely rich conditions (Φ>5.0) are not available in the literature, and hence the performance of these mechanisms at these conditions is unknown.

The goal of developing a chemical kinetic model for biofuels is to use it in engine or combustor simulations. It is well known that engines and combustors have zones with low mixing or less efficient combustion with high equivalence ratios[31]. This partially mixed fuel can be exposed to high-temperature zones and create high temperature and extremely rich combustion. In this work, we conducted high temperature (1700-2100 K) extremely rich oxidation (Φ= 8.6) of ethylene and five Co-optima biofuel blends with ethylene. We measure carbon monoxide and ethylene time-histories as both are important combustion intermediates at these conditions. Carbon monoxide is also a good indicator of combustion efficiency, while ethylene time history shows how much of the parent molecule gets converted to ethylene in the first few microseconds. Accurately capturing their time histories will help validate chemical kinetic models

used to design and develop engines and combustors with improved combustion efficiencies. Laser absorption spectroscopy was used to measure carbon monoxide and ethylene time histories behind reflected shock waves, and comparative analysis was made using the results obtained. Results obtained were compared with recent mechanisms from literature, and their performance at our experimental conditions was assessed. Pathway analysis was also conducted using the Co-Optima mechanism to highlight the crucial pathways leading to carbon monoxide and ethylene at high temperatures and extremely rich conditions.

2. Experimental methods

2.1. Shock tube facility

Experiments were conducted in the shock tube facility located at the University of Central Florida (UCF). The UCF shock tube is constructed out of stainless steel tube with an inside diameter of 0.14 m and can be heated up to 493 K using custom-built heating jackets. The test section is located 2 cm away from the end wall on the driven side. The test section has six optical ports for spectroscopic measurements and two pressure transducers (Kistler 603B1 and PCB 113B26) for accurate pressure measurements. The diaphragm used in this work is a polycarbonate resin thermoplastic (Lexan) with a thickness of 0.38 mm and separates the driven and driver side of the shock tube. Before each experiment, the driven side was vacuumed to 5 x 10^{-5} torr using a combination of a rotary vane pump (Agilent DS102) and a turbo molecular pump (Agilent V301). The driver side was vacuumed using a separate rotary vane pump (Agilent DS102). After filling the driven side with a test gas mixture to desired pressure (P_1), the driver side is pressurized using helium. The pressure exerted by helium breaks the diaphragm, creating a shockwave that propagates down the length of the driven side, heating the test gas mixture on its path. Upon hitting the end wall, the shock wave reflects and heats the test mixture to post-shock temperature (T_5) and pressure (P_5). In order to measure the shock wave velocity at the end section, the driven side is equipped with five equally spaced piezoelectric pressure transducers (PCB 113B26) and time interval counters (Agilent 53220A) which triggers upon arrival of the shock wave. The velocities obtained using timer counter values are then extrapolated to get the shock wave velocity at the test section. Using this velocity in the one-dimensional shock equation, the uncertainties in post-shock temperature and pressure were estimated to be less than 2% and 1.8%, respectively. More details on the shock tube facility can be found in our recent works[30, 32-38].

2.2. Mixture preparation

The test mixture was prepared in a 33 L Teflon coated stainless steel tank which can be heated up to 493 K. The mixtures were prepared utilizing Dalton's law using a 100 torr manometer (MKS Baratron E27D) and a 10000 torr manometer (MKS 628D). Before preparing the mixture, the mixing tank was vacuumed to $5x10^{-5}$ torr. The mixing tank was at ambient temperature for mixtures with only gaseous fuels. For blends involving liquid fuels, the mixing tank was heated to 393 K. The liquid fuel was injected into the tank, followed by ethylene, oxygen, and argon. Argon, oxygen, and ethylene were of 99.999% purity or higher obtained from NexAir. Other biofuels used in this work were: 2,4,4-trimethyl-1-pentene or α-diisobutylene (99%), 2-methylfuran (99%), and ethanol (99.5%) from Acros organics, cyclopentanone (99%), and methyl acetate (99%) from Alfa Aesar. The mixture was left to mix for at least 3 hours using a magnetically driven stirrer to ensure homogeneity. Different mixtures used in this work and their compositions are shown in Table 1.

Table 1: Experimental reactant compositions investigated (X=mole fraction, ϕ = equivalence ratio)

Mixture	Biofuel	Chemical Formula	$X_{biofuel}$	X_{C2H4}	X_{O2}	ϕ	Carbon content (% vol)
1[a]	-	-	-	0.0250	0.0087	8.6	5
2	α-diisobutylene	C_8H_{16}	0.0016	0.0188	0.0083		
3	Ethanol	C_2H_5OH	0.0063	0.0188	0.0087		
4	Cyclopentanone	C_5H_8O	0.0025	0.0188	0.0084		
5	Methyl acetate	$C_3H_6O_2$	0.0042	0.0188	0.0082		
6	Methylfuran	C_5H_6O	0.0025	0.0188	0.0087		

[a] Baseline mixture containing only ethylene, oxygen, and argon for comparison purpose.

2.3. Laser absorption spectroscopy

Carbon monoxide (CO) was measured using a continuous feedback quantum cascade laser (Alpes Lasers (TO3-L-50) centered at 2046.277 cm^{-1} (4.9 µm). The CO concentration time-histories are obtained using the equation:

$$X_{CO} = \frac{ln\left(\frac{I_0}{I_t}\right)_{CO} * \mathrm{RT_5}}{\sigma_{CO} \mathrm{P_5} L} \quad (1)$$

Here, I_o and I_t are the reference and transmitted intensities from the laser, L is the absorbing path length, and σ_{CO} is the absorption cross-section of CO at reflected T_5 and P_5 obtained from the HITRAN[39] database.

Ethylene (C_2H_4) was measured using a tunable CO_2 gas laser (Access Laser L4GS) at 949.49 cm^{-1}. Figure 1 shows the absorbance by major species (predicted to be important by the Co-Optima model) at 1750 K and 4.5 atm at this wavelength. Since large hydrocarbons break into smaller ones at high temperatures, water is a probable interfering species. Thus, we used the ethylene-ethanol blend as it forms more water than other biofuel blends because of the water elimination reaction of ethanol. It can be seen that the interference from other species is negligible under these conditions.

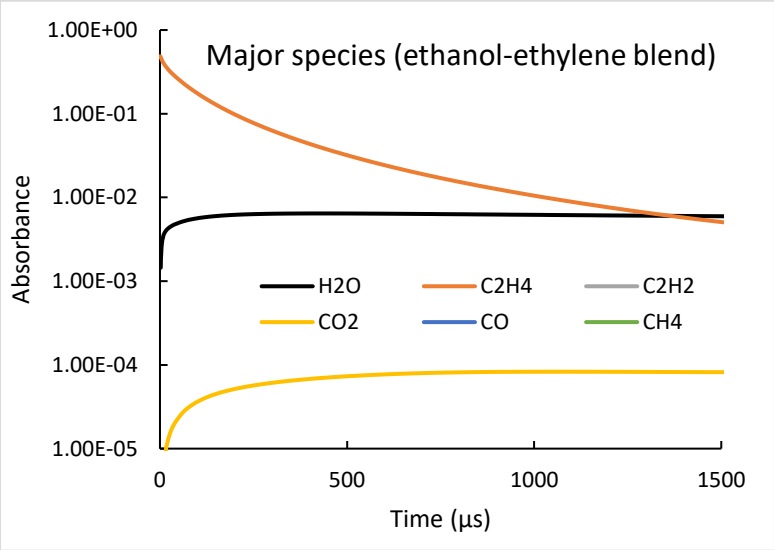

Figure 1. Simulated absorbance vs. time for major species formed during oxidation of ethanol-ethylene blend at 1750 K and 4.5 atm at equivalence ratio 8.6.

The C_2H_4 concentration time-histories are obtained using the equation:

$$X_{C2H4} = \frac{ln\left(\frac{I_0}{I_t}\right)_{C2H4} * \mathrm{RT_5}}{\sigma_{C2H4}\mathrm{P_5}L} \qquad 2$$

Here, σ_{C2H4} is the cross-section of ethylene at T_5 and P_5 obtained using the correlation from Ren et al.[40].

The uncertainty in mole fraction is calculated as following

$$\frac{\delta X}{X} = \sqrt{\frac{\delta P}{P} + \frac{\delta T}{T} + \frac{\delta L}{L} + \frac{\delta \sigma}{\sigma}}$$

Uncertainty in post-shock pressure and temperature were calculated from experimental apparatuses (timer counters, initial driven side pressure, initial temperature, manometers for mixture preparation, etc.). Uncertainty in optical path length (L) was obtained by direct measurement using measuring tools in our facility. Uncertainty in absorption cross-section includes the uncertainty due to changes in temperature and our facility effects. When all these uncertainties are accounted for, mole fraction uncertainties for CO and C_2H_4 are less than 10 %. Further details about the measurement procedure can be found in our previous work [41].

3. Modeling methods

The temperature changes in the shock tube from a pre-shock temperature T_1 (~298-393 K) to post-shock temperature T_5 (~1600-2100 K) occur in a few microseconds. Hence, it can be approximated to be a step-change in temperature, which helps model the system with an initial temperature of T_5. Since the mixture inside the shock tube is homogeneous (mixed for at least 3 hours in the mixing tank), 0-D homogeneous reactor simulations were conducted. As the post-shock pressure was constant throughout the test time, simulations were performed assuming constant pressure. During the test time (~2 ms), the heat transfer to the surroundings is negligible. This helps in assuming the reactor to be adiabatic. The only energy change would be due to the energy consumed or released by chemical reactions in the system. Hence, all simulations were conducted using a constant pressure 0-D closed homogeneous reactor in Chemkin-Pro using the energy solver module without any energy transfer to surroundings.

4. Results and discussion

4.1. Shock tube data:

Figure 2 shows the carbon monoxide and ethylene time-histories measured during rich oxidation of ethylene and its blend with α-DIB. In general, the CO mole fraction rises steeply initially and then continues to increase gradually throughout the test time (1.5 ms). With an increase in temperature from ~1700 K to ~2000 K, an increase in the amount of CO formed is higher for mixture 1 than mixture 2. Ethylene time history shows a gradual consumption, eventually resulting in all ethylene in the mixture being converted to other species in less than 1 ms for both mixtures 1 and 2.

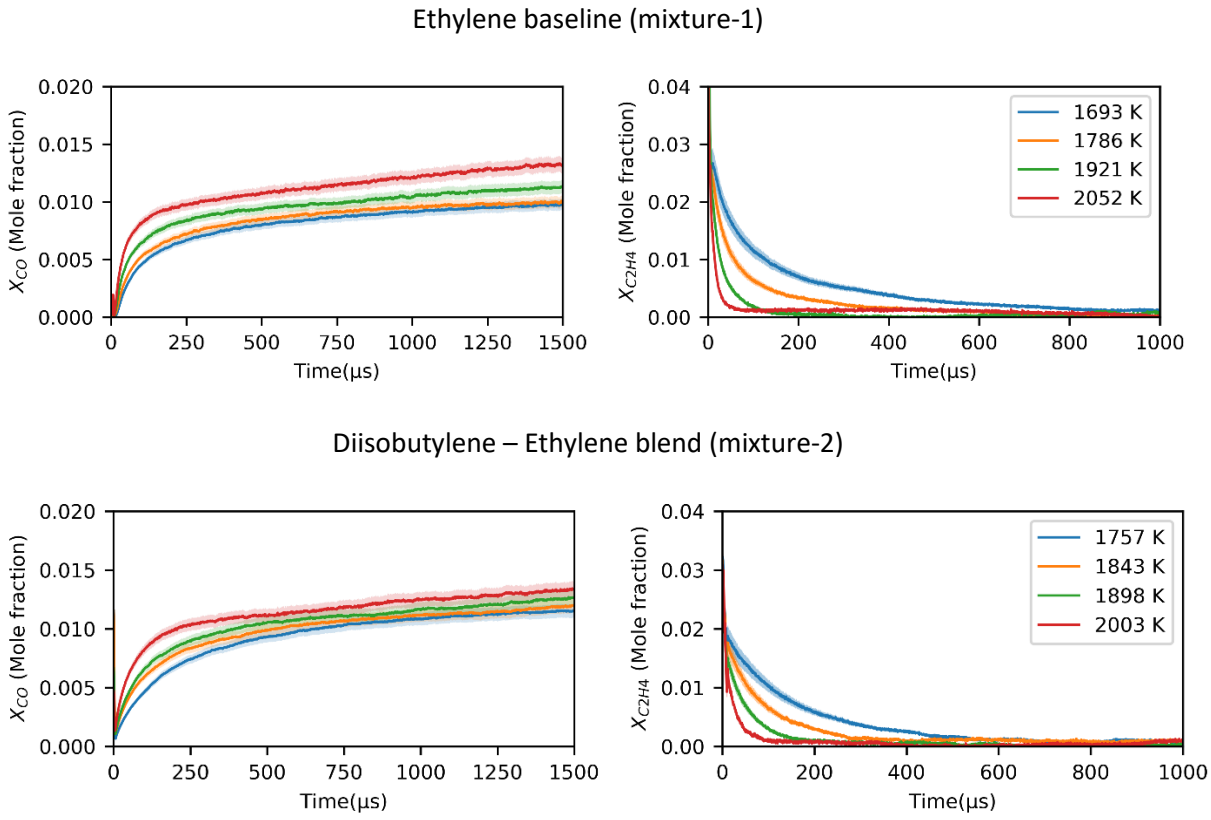

Figure 2. Carbon monoxide and ethylene time-histories during the oxidation (ø=8.6) of baseline ethylene mixture 1 and DIB blend mixture 2.

Figure 3 shows the CO and ethylene time-histories for blends of ethylene with oxygenated biofuels, namely ethanol, cyclopentanone, methyl acetate, and 2-methylfuran. Similar to mixture -1 and -2, these mixtures also have a sharp increase in CO mole fraction in the first 0.25 ms and then gradually increase until the end of test time. Additionally, an immediate rise in CO near time zero has been observed for these oxygenated biofuel blends. These can be attributed to the fuel-specific reactions that contribute to the formation of CO as discussed in the following sections As clearly evident, methyl acetate and ethanol produce more CO than any other mixtures under these conditions. The C_2H_4 time-histories show a gradual consumption profile until it is fully consumed or converted to other species for all oxygenated mixtures.

Ethanol – Ethylene blend (mixture-3)

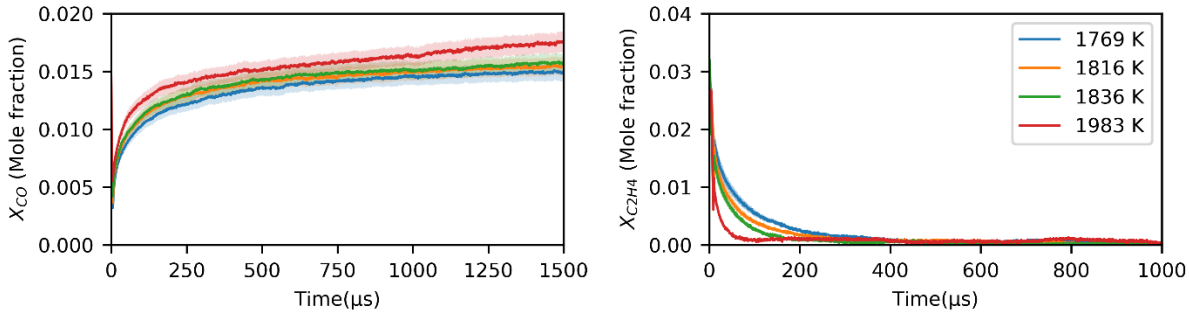

Cyclopentanone – Ethylene blend (mixture-4)

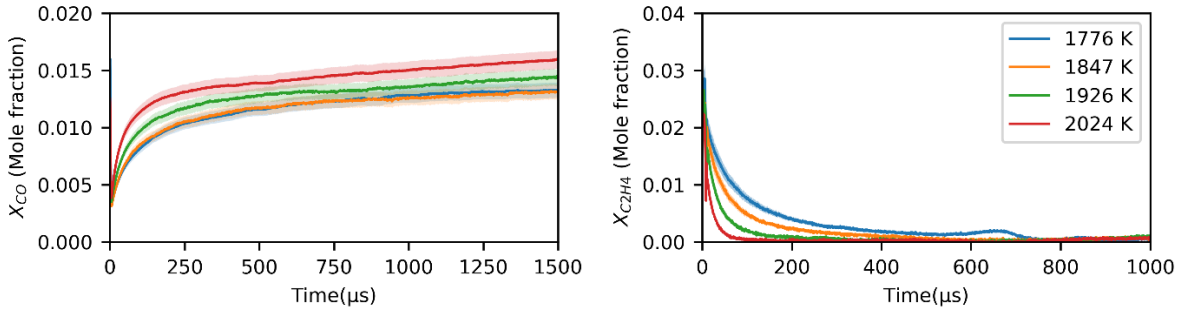

Methyl acetate – Ethylene blend (mixture-5)

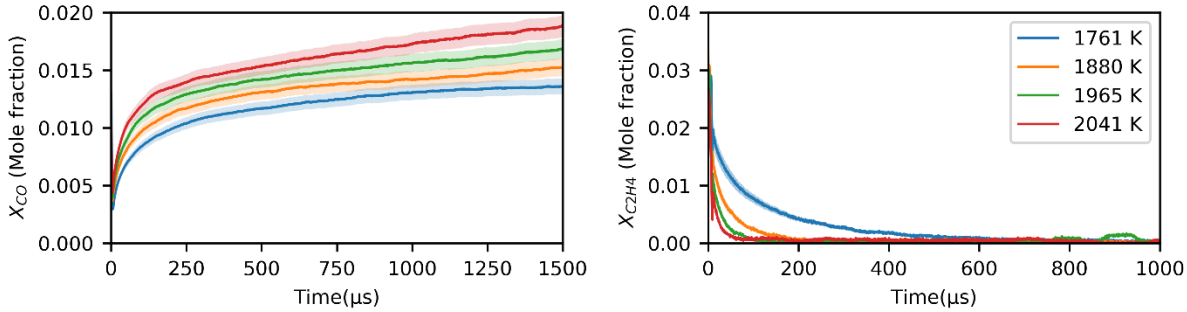

Methylfuran – Ethylene blend (mixture-6)

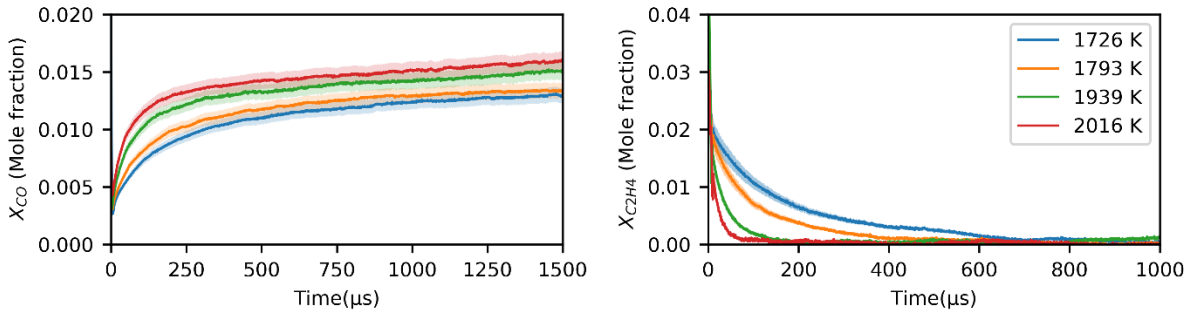

Figure 3. Carbon monoxide and ethylene time-histories during oxidation of oxygenated fuel blends at equivalence ratio 8.6

To compare the CO and ethylene time-histories more effectively for each biofuel, they were plotted in figure 4 at a common temperature. At 1800 K, CO formation is highest for ethanol blend and produces an approximately 1.5-mole percentage of carbon monoxide by the end of test time. Other oxygenated biofuels have almost the same CO formed with methyl acetate blend producing slightly higher CO followed by methylfuran and cyclopentanone blends. Diisobutylene blend and ethylene have the same amount of CO formed during the first 0.2 ms, after which diisobutylene blend diverges and produces more CO. C_2H_4 consumption is slowest for diisobutylene and fastest for ethanol blend. The slow consumption of ethylene in the diisobutylene blend can be attributed to the formation of ethylene during the breakage of diisobutylene. Faster conversion of ethylene in ethanol blend than ethylene baseline case may be due to the increased presence of OH radical during the dissociation of ethanol molecule by reaction $C_2H_5OH = C_2H_5 + OH$, thereby enhancing reaction progress. Higher CO formation for ethanol and other oxygenated biofuel blends indicates that oxygen in the biofuel molecule enhances oxidation, reducing soot formation, as observed in Barak et al.[30]. Even though CO formed from the diisobutylene blend is more than the ethylene baseline mixture, the larger diisobutylene molecule produces more propargyl radicals (refer Fig. 12) during combustion, which can explain the higher soot formation observed for the diisobutylene blend in Barak et al.[30].

Similar trends are observed at 2000 K (see Figure 4) for CO time-histories with all mixtures except the methyl acetate blend. Till 0.5 ms, CO produced from mixtures containing methyl acetate, cyclopentanone and methylfuran coincide with each other, while at later times, the rate of CO production is higher for methyl acetate blend. C_2H_4 time-histories at 2000 K show that C_2H_4 in all of these mixtures is consumed at a similar rate at this temperature.

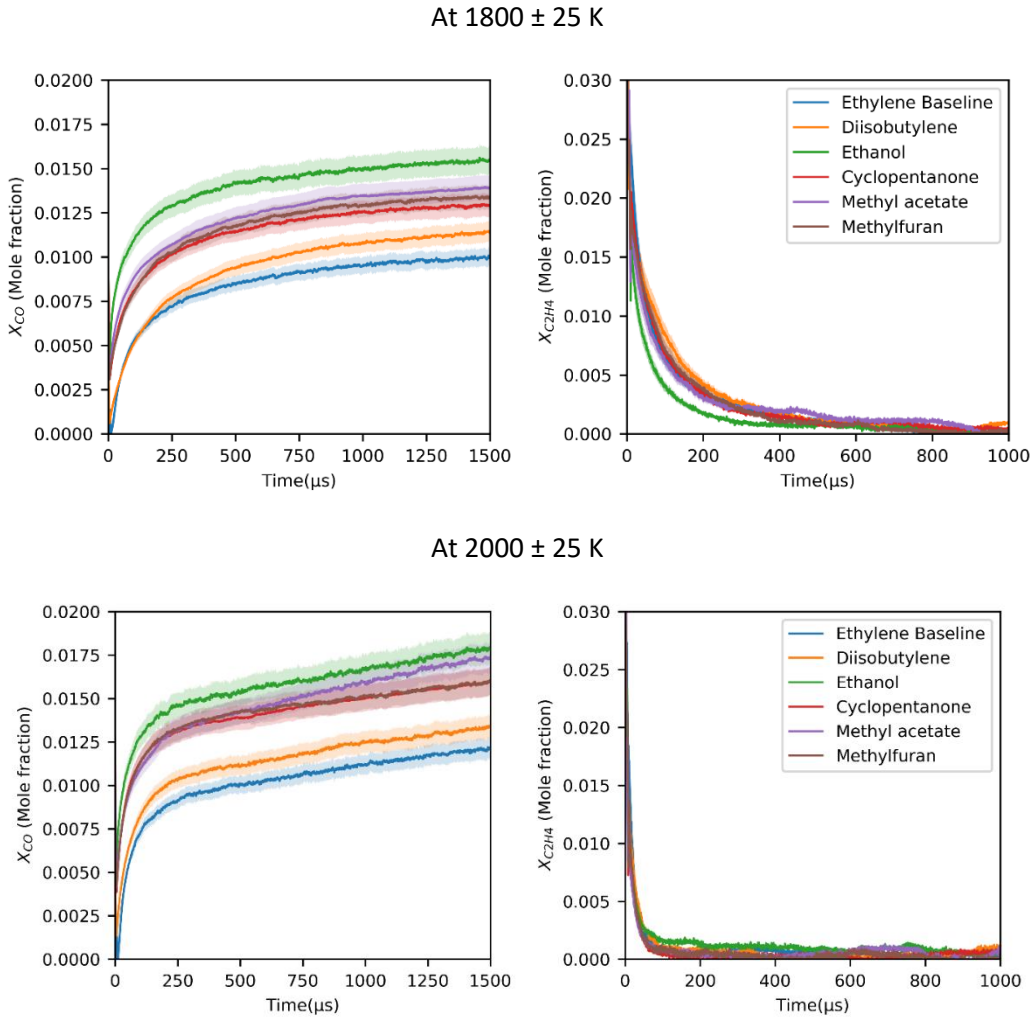

Figure 4. Carbon monoxide and ethylene time-histories during oxidation of Co-Optima fuels near 1800 K and 2000 K at equivalence ratio 8.6.

4.2. Comparison with models

The experimental data obtained for rich oxidation of ethylene baseline mixture were used to evaluate the performance of some of the n-alkene mechanisms available in the literature. The simulation results obtained for CO and ethylene mole fraction time-histories using Aramco 3.0[42], CRECK model[43], and Jetsurf 2.0[44] mechanism, and experimental results obtained in this work are shown in Figure 5. We also show the results obtained with the latest version of the Co-Optima model. At 1750 K and 1989 K, all models capture the general trend in the growth of carbon monoxide mole fraction and ethylene decay. Aramco 3.0 and Co-Optima models predict CO and C_2H_4 profiles within experimental uncertainty at 1750 K, while CRECK and Jetsurf 2.0 over predicts CO formation and C_2H_4 decay at this temperature. At 1989 K,

ethylene mole fraction time-history predictions are satisfactory with all models while CO is over predicted by the CRECK model.

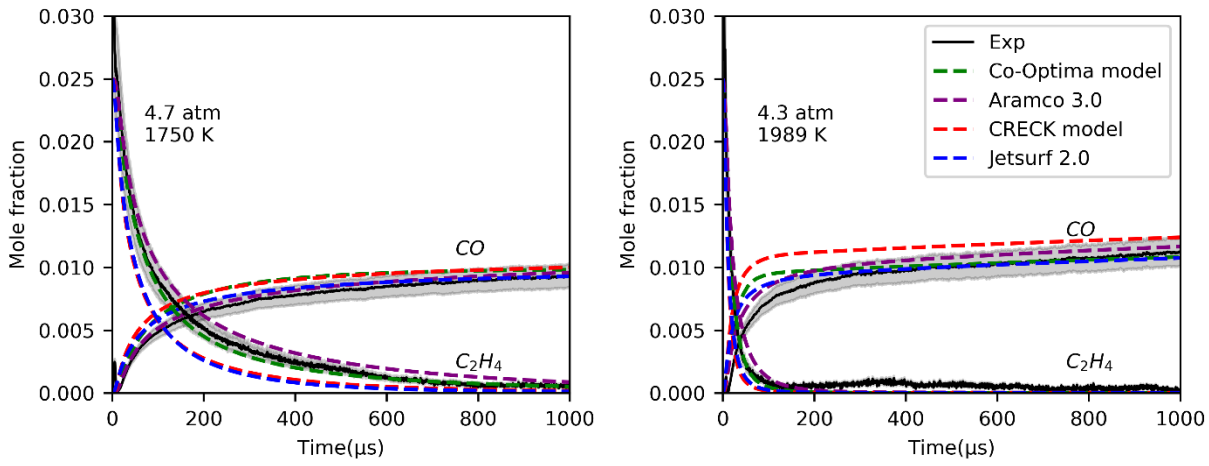

Figure 5. Performance of recent mechanisms from the literature on predicting carbon monoxide and ethylene time-histories during oxidation of ethylene baseline mixture 1 at equivalence ratio 8.6. Shaded region shows experimental uncertainty.

Two recent mechanisms from literature and the Co-Optima model were compared with the experimental results obtained from shock tube experiments in this work. It can be seen that both Metcalfe et al.[8] and Li et al.[10] over predict CO formation and ethylene decay during the first 600 microseconds (Figure 6). This shows that the H atom consumption reactions during the initial 600 microseconds are not well defined in these mechanisms. However, the Co-Optima mechanism captures the initial growth of CO and decay of C_2H_4 within the uncertainty of experiments. At 2003 K, all three mechanisms are able to capture ethylene decay mole fraction satisfactorily while CO formation during initial 100 microseconds needs some improvement. It is also observed that the Co-Optima model predicts lower CO mole fraction than other models and experiments.

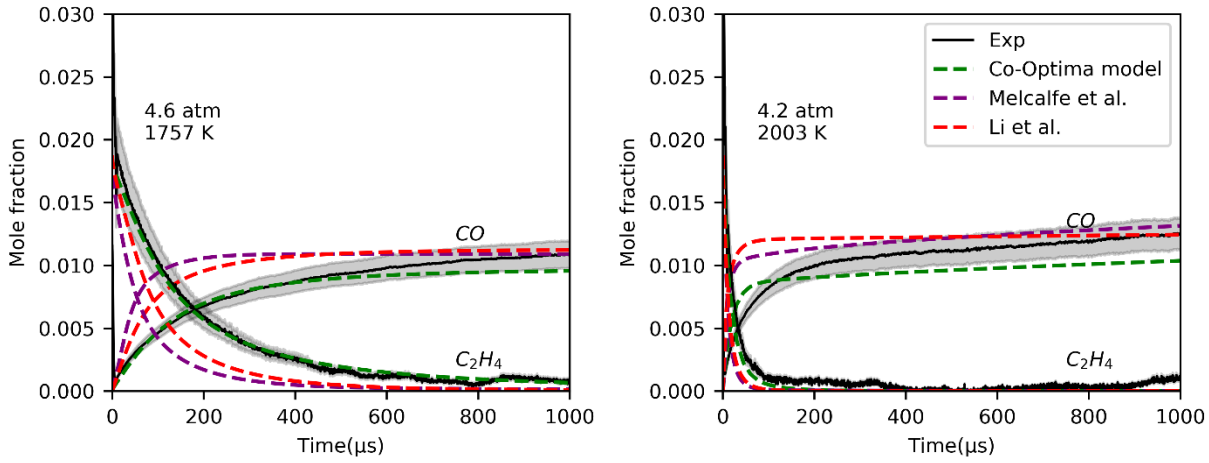

Figure 6. Performance of recent mechanisms from the literature on predicting carbon monoxide and ethylene time-histories during oxidation of diisobutylene-ethylene blend at equivalence ratio 8.6. Shaded region shows experimental uncertainty.

Figure 7 compares experimental results for CO and C_2H_4 mole fraction time-histories with different models from literature for the ethanol-ethylene blend. The comparisons are shown against Aramco 3.0 mechanism, the C_1-C_3 alcohol mechanism by Frassoldati et al.[45], the alcohol combustion chemistry model from Sarathy et al.[11], and the Co-Optima model. The Co-Optima model predicts CO mole fraction time-histories better than other models shown in Figure 7 at 1769K. The decay in C_2H_4 is slower with this model than the experimental results at this temperature. At 1988 K, ethylene decay is predicted satisfactorily by all models. Predictions by both Sarathy et al. and Aramco 3.0 models deviate from experimental CO time-history near 100 microseconds. In contrast, Frassoldati et al. and the Co-Optima model starts to deviate from experimental CO results close to 150-200 microseconds.

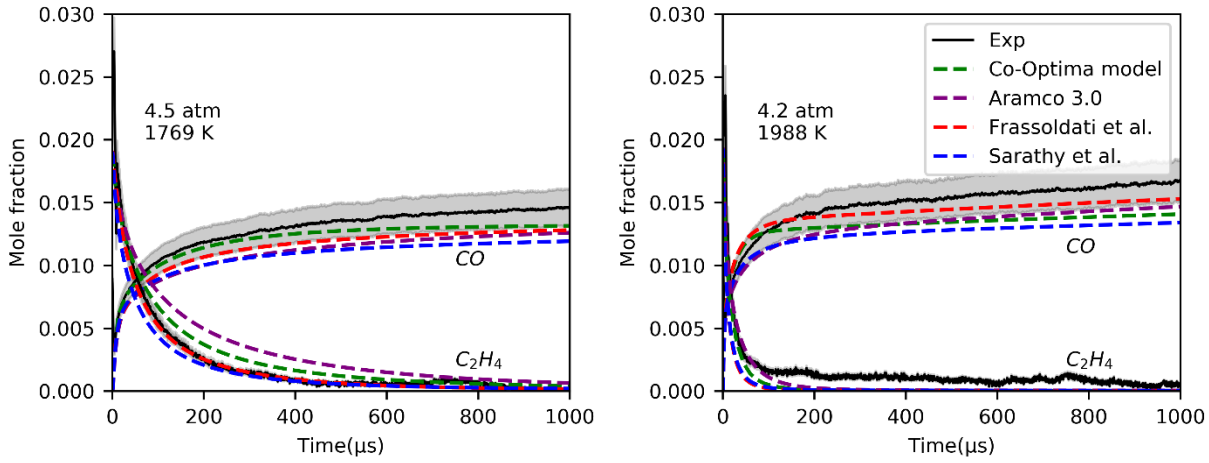

Figure 7. Performance of recent mechanisms from the literature on predicting carbon monoxide and ethylene time-histories during oxidation of ethanol-ethylene blend at equivalence ratio 8.6. Shaded region shows experimental uncertainty.

CO and C_2H_4 mole fraction time-histories obtained from rich oxidation of cyclopentanone-ethylene blend were compared against Thion et al.[20], Zhang et al.[18], and the Co-Optima models in Figure 8. At 1776 K, both Thion et al. and Zhang et al. over-predicted ethylene decay while CO formation was over predicted by Thion et al. and under predicted by Zhang et al. model. At 1971 K, CO and C_2H_4 mole fraction time-histories are predicted within uncertainties by all three models.

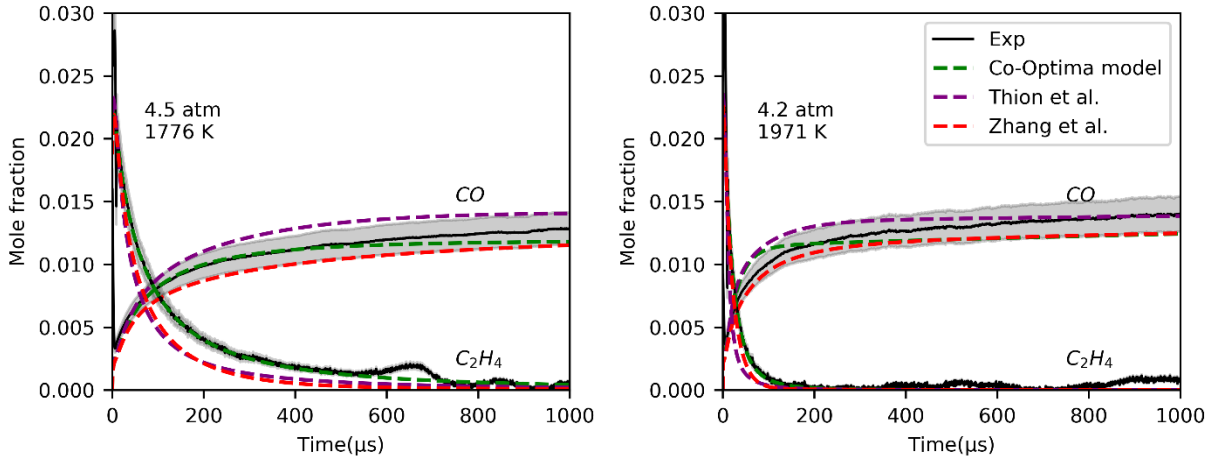

Figure 8. Performance of recent mechanisms from the literature on predicting carbon monoxide and ethylene time-histories during oxidation of cyclopentanone-ethylene blend at equivalence ratio 8.6. Shaded region shows experimental uncertainty.

The experimental results for CO and C_2H_4 mole fraction time-histories during oxidation for the methyl acetate-ethylene blend at 1761 K and 2005 K were compared against Ahmed et al.[24] and Co-Optima models (Figure 9). Results show that the Co-Optima model captures CO formation and ethylene decay time-histories within the uncertainty of experiments at 1761 K. Ahmed et al.[24] mechanism under predicts both CO formation and ethylene decay time-histories under these conditions. At higher temperatures (2005 K), both Co-Optima and Ahmed et al. captures C_2H_4 time-histories accurately while CO formation time-histories are under-predicted by both models.

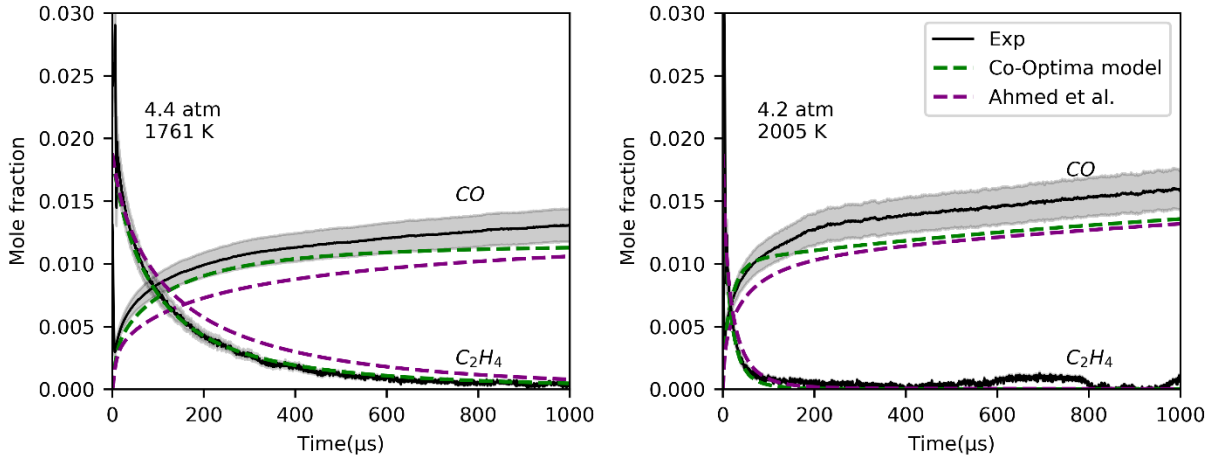

Figure 9. Performance of recent mechanisms from the literature on predicting carbon monoxide and ethylene time-histories during oxidation of methyl acetate-ethylene blend at equivalence ratio 8.6. Shaded region shows experimental uncertainty.

Time-histories of CO and C_2H_4 mole fractions obtained during fuel-rich oxidation of methylfuran-ethylene blend were compared against predicted results from Cheng et al.[46], Tran et al.[29], Somers et al.[26], and Co-Optima model (Figure 10). At 1760 K, the Co-Optima model predicts CO and C_2H_4 mole fraction time-histories within experimental uncertainty. At this temperature, CO formation is under-predicted by both Chen et al. and Somers et al. model while Tran et al. over predict CO formation. At 1974 K, a sharp deviation in CO mole fraction is observed within the first 150 microseconds by the Tran et al. model, while all other models capture the trend in CO growth during this time. After 200 microseconds, CO predicted by the Tran et al. model moves closer to experimentally observed CO while other models move away from experimentally observed CO.

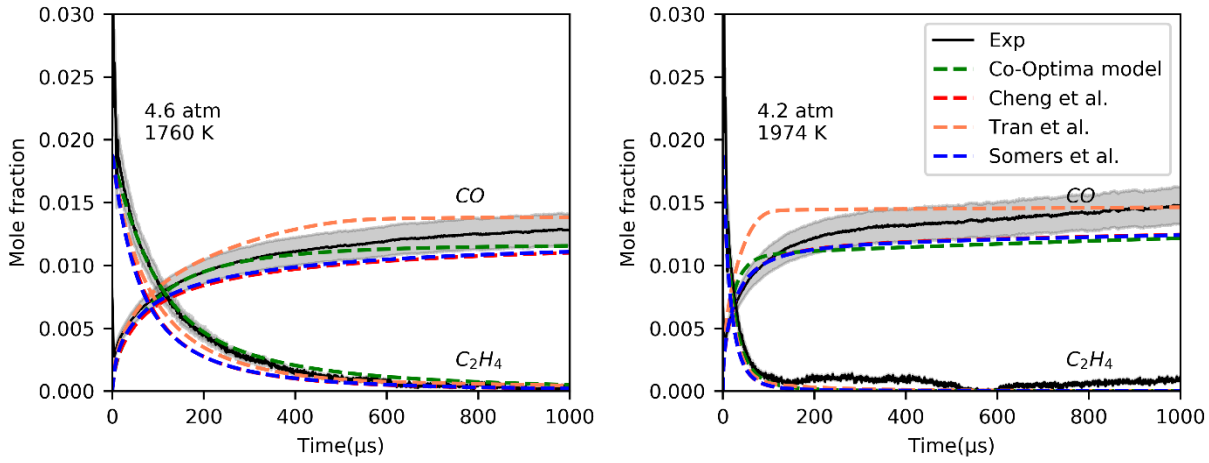

Figure 10. Performance of recent mechanisms from the literature on predicting carbon monoxide and ethylene time-histories during oxidation of 2-methylfuran-ethylene blend at equivalence ratio 8.6. Shaded region shows experimental uncertainty.

4.3. Reaction Pathway Analysis:

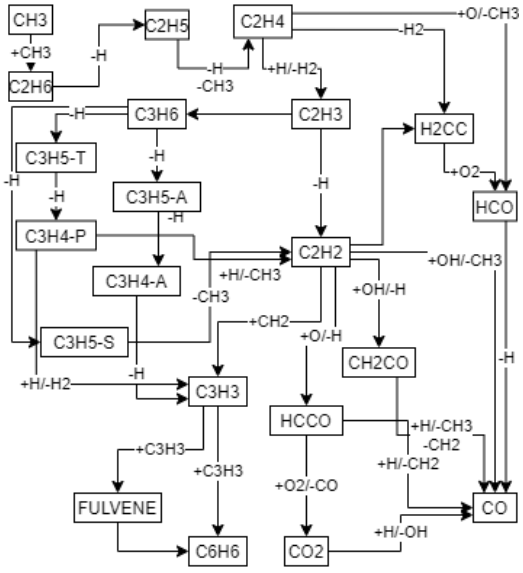

Figure 11. Major reaction pathways during oxidation of ethylene baseline mixture at 1800 K and equivalence ratio 8.6.

Figure 11 shows the major reaction paths for ethylene oxidation at equivalence ratio 8.6 using the Co-Optima model. Initiation of ethylene reactions starts with the reaction R1 and R2. The vinylidene radical formed in reaction R1 reacts with oxygen to form HCO, disintegrating to CO and H atoms. This CO production is visible as the steep increase in CO during the first 250 microseconds.

C2H4 (+M)=H2 +H2CC (+M) R1

C2H4(+M)=C2H3+H (+M) R2

Reaction R2 increases the concentration of H atoms in the system and eventually initiates the reactions R3, R4, and R5. The vinyl radical formed undergoes dissociation to give more H atoms by reaction R3.

C2H3 (+M)=C2H2+H (+M) R3

C2H4+H=C2H3+H2 R4

O2+H=O+OH R5

R4 abstracts H atoms from ethylene and forms vinyl radical and hydrogen. At the same time, R5 is the well-known high-temperature chain branching reaction in an oxidizing environment that produces radicals O and OH. Since R4 and R5 competes for H atoms during this stage, the rate of reaction of R4 plays an important role in the initial decomposition steps of ethylene. Due to this, this reaction is studied experimentally[47, 48] and theoretically[49, 50] by several works. In the Co-Optima model, the rate by Knyazev et al.[49] is used for this reaction as in Aramco 3.0.

Under rich conditions, the methyl radical formed recombines to form ethane and subsequently forms ethylene by losing hydrogen atoms, as shown in reactions R6-R8.

CH3+CH3 (+M)=C2H6 (+M) R6

C2H6 (+M)=C2H5+H (+M) R7

C2H5 (+M)=C2H4+H (+M) R8

One of the significant products during the fuel-rich combustion of ethylene is acetylene (C2H2). Acetylene is relatively stable at our experimental conditions (~1600 – 2100 K and ~4-5 atm). It undergoes slow reactions with radicals OH and O to form CO. It also undergoes rearrangement to vinylidene (H2CC) radical followed by reaction with oxygen to form carbon monoxide formation, as shown in Figure 11. The CO formation from acetylene through these pathways is slow and evident in the experimental results at time greater than 250 microseconds. Since other biofuels discussed in this work also form ethylene at high temperatures, the acetylene pathways shown in Figure 11 are also applicable for ethylene formed from these biofuels.

Figure 12a shows the major reaction pathways during the oxidation of α-DIB-ethylene blend at equivalence ratio 8.6.

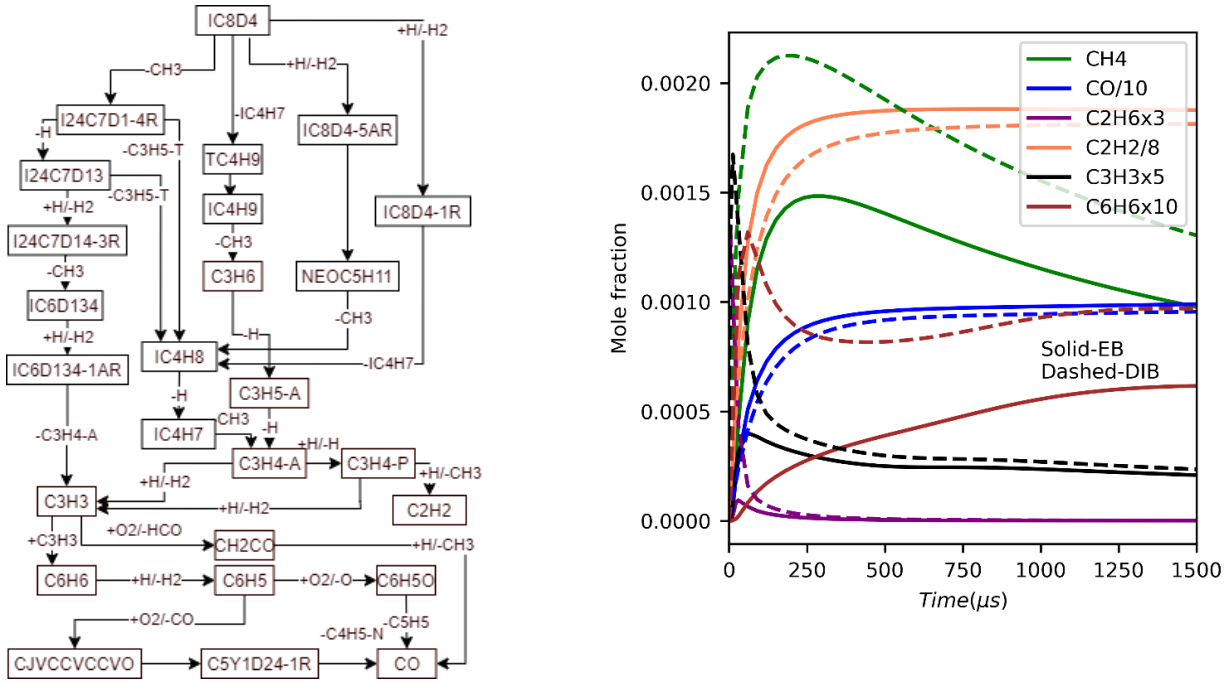

Figure 12. a) Major reaction pathways during oxidation of α-DIB -ethylene baseline mixture at 1800 K and equivalence ratio 8.6, b) Simulated time-histories of major species formed under this condition (DIB) compared to the ethylene-baseline mixture (EB) using the Co-Optima model.

α-DIB (IC8D4) decomposes to IC4H7 and TC4H9 at high temperature by reaction R9 and then proceeds eventually to form propargyl radical and acetylene through subsequent reactions shown in Figure 12a.

IC8D4=TC4H9+IC4H7 R9

Other important decomposition pathways for α-DIB at high temperatures are the elimination of methyl radical and the H-abstraction reactions by H atoms shown in Figure 12a. All these pathways eventually result in the formation of more propargyl radicals. Since propargyl and acetylene are important intermediates in the growth of polycyclic aromatic hydrocarbons, more soot was observed for the α-DIB blend, as stated in Barak et al.[30]. The methyl radical released during the reaction R10 recombines and forms ethane and then ethylene, as shown in R6-R8.

C3H4-P+H=C2H2+CH3 R10

Figure 12b shows the simulated mole fraction time-histories for α-DIB blend and ethylene baseline at 1800 K using the Co- optima model. It is clear that more amounts of methane, ethane, propargyl, and benzene are formed in the diisobutylene blend than in the ethylene baseline. However, the model shows less acetylene formed from the diisobutylene blend during the first 1.5 ms. Since the diisobutylene blend considered here has a considerable amount of ethylene (1.875-mole %), most of the CO production is

primarily through the pathway shown in Figure 11 for ethylene and acetylene. Additionally, more propargyl and phenyl radical (from benzene) formed in the initial 100 μs for α-DIB blend also contributes to the formation of CO by the reactions R11-R16.

C3H3+O2=CH2CO+HCO	R11
C6H5+O2=CJVCCVCCVO+CO	R12
C6H5+O2=C6H5O+O	R13
C6H5O=C5H5+CO	R14
CJCCVCCVO=C5Y1D24-1R	R15
C5Y1D24-1R=C4H5-N+CO	R16

Figure 13a shows the major reaction pathways leading to CO and C_2H_4 during the rich oxidation of ethanol blend at equivalence ratio=8.6. Major unimolecular decomposition of ethanol involves the elimination of methyl radical, water, or hydroxyl radical by reactions R17-R19. Reaction R18 produces ethylene and R19 produces ethyl radical, which eventually produces ethylene by reaction R8.

C2H5OH=CH3+CH2OH	R17
C2H5OH=C2H4+H2O	R18
C2H5OH=C2H5+OH	R19

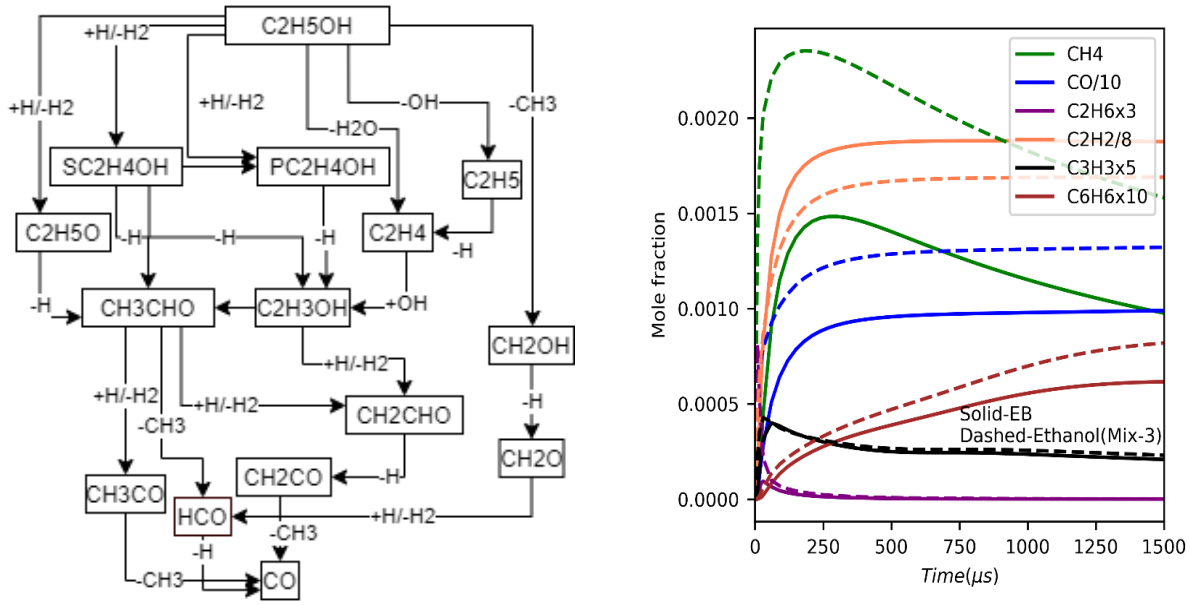

Figure 13.a) Major reaction pathways during oxidation of ethanol-ethylene baseline mixture at 1800 K and equivalence ratio 8.6, b) Simulated time-histories of major species formed under this condition compared to the ethylene-baseline mixture.

The reaction R17 produces CH2OH, which loses one H atom to form formaldehyde. Formaldehyde then undergoes H abstraction by H atom to form HCO, which releases CO and H atoms. This process is fast and the CO formed through this pathway is responsible for the immediate increase in CO mole fraction time-histories near time zero. Other important reactions for ethanol under high temperature and fuel-rich conditions include H- abstraction by hydrogen atoms, as shown in Figure 13a. The radicals formed from these reactions lose H-atoms to form acetaldehyde (CH3CHO), and subsequent reactions lead to carbon monoxide formation. The role of these radicals in the formation of CO was also studied in our previous work[14]. Apart from this pathway, CO is also produced from ethylene formed from ethanol through pathways shown for the ethylene baseline mixture (Figure 11). The higher amount of CO formed from the ethanol blend than the ethylene baseline mixture (Figure 13b) is attributed to the C bonded to O that is present in the molecular structure of ethanol but absent in the molecular structure of ethylene. The C-O in ethanol's structure is retained when it forms CH2OH/CH3CHO, leading to carbon monoxide (CO). In addition to CO, Figure 13b shows more methane and benzene is observed for ethanol blend at 1800 K. Increase in methane concentration is attributed to the methyl radicals formed during the intermediate reactions R20-R22 and its conversion to methane by reaction R23. Additionally, methyl radicals formed from these reactions also recombine and form more ethylene through reaction R6-R8.

CH2CO+H=CH3+CO	R20
CH3CO (+M)=CH3+CO (+M)	R21
CH2CHO (+M)=CH3+CO (+M)	R22
CH3+H (+M)=CH4 (+M)	R23

Acetylene formed from ethanol blend is lower than baseline mixture while propargyl formed remains almost the same as baseline mixture.

Figure 14a shows the major reaction pathways during rich oxidation of cyclopentanone blend at equivalence ratio 8.6. The most dominant reaction of cyclopentanone is the unimolecular decomposition to form ethylene and carbon monoxide, as shown in reaction R24. CO formed by this reaction causes an immediate increase in CO mole fraction near time zero as evident in our experimental results (Fig.3). Other reactions include the rearrangement of cyclopentanone and H abstraction reactions, as shown in R25-R27.

CPN=>2C2H4+CO	R24
CPN=C4H7CHO-4	R25

CPN+H=CPN-2R+H2 R26

CPN+H=CPN-3R+H2 R27

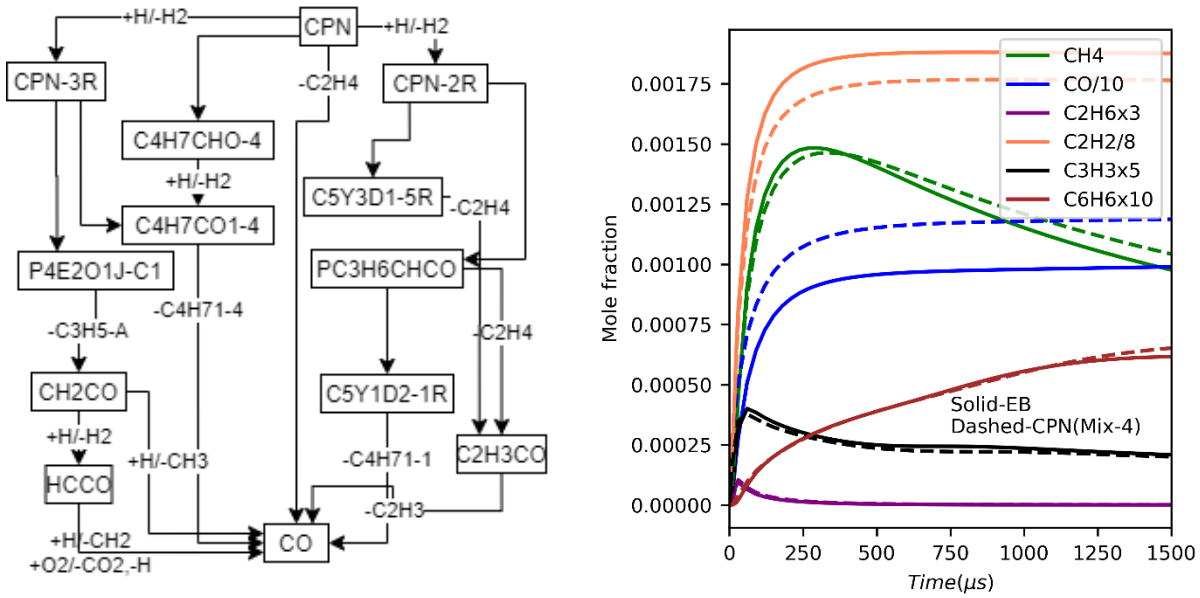

Figure 14. a) Major reaction pathways during oxidation of cyclopentanone-ethylene baseline mixture at 1800 K and equivalence ratio 8.6, b) Simulated time-histories of major species formed under this condition (CPN) compared to the ethylene-baseline mixture (EB).

As shown in figure 14a, many of the intermediate reactions of cyclopentanone produce ethylene as a product. The decomposition and oxidation of ethylene proceeds similar to the baseline mixture (Figure 11). Figure 14b shows the simulated results for some of the hydrocarbon species and CO formed during the cyclopentanone blend and ethylene baseline mixture. It can be seen that methane, ethane, propargyl, and benzene concentrations are almost the same with both mixtures. The reduction observed for acetylene with cyclopentanone blend can be attributed to the increased conversion of cyclopentanone to CO by reaction R24.

Figure 15a shows the major pathways through which methyl acetate is consumed during fuel-rich oxidation of methyl acetate blend. Figure 15b shows the simulated results for important species during oxidation of methyl acetate blend compared to ethylene baseline mixture. Most of the methyl acetate in the mixture gets consumed through the unimolecular decomposition reactions R28 and R29 releasing methyl group.

CH3COOCH3=CH3CO2+CH3 R28

CH3COOCH3=CH3OCO+CH3 R29

The products of these reactions, CH3CO2 and CH3OCO, decompose to produce methyl radical and carbon dioxide. This results in a sudden increase in methane and carbon dioxide concentration in the initial 100 µs, as shown in Figure 15b. This immediate increase in CO mole fraction is also evident in the experimental results (Fig.3). Since the conversion of CO to CO2 is relatively slow for conditions relevant to current experiments (fuel-rich and dilute), it is clear that more than 75% of methyl acetate present in the mixture decomposes through this pathway at 1800 K. Additionally, the rates for these reactions are obtained from Peukert et al. [51] and does not show any fall-off near 2000 K. Future work is needed to investigate its fall-off at high temperatures and the rate constants near 2000 K. Other pathways for consumption of methyl acetate includes unimolecular decomposition to form methanol and H-abstraction reactions by H atoms. All these pathways lead to more CO and methyl radicals, as shown in Figure 15a.

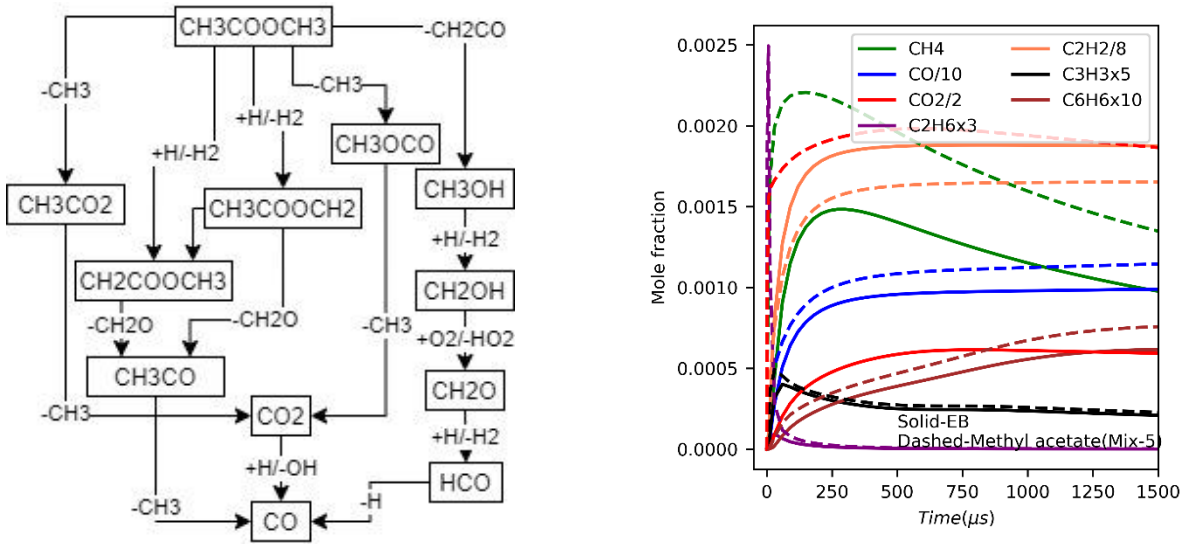

Figure 15. a) Major reaction pathways during oxidation of methyl acetate-ethylene baseline mixture at 1800 K and equivalence ratio 8.6, b) Simulated time-histories of major species formed under this condition compared to the ethylene-baseline mixture (EB).

The sudden increase in concentration and consumption of ethane within the initial 100 µs (Figure 15b) indicate the role of recombination of methyl radicals produced from the unimolecular decomposition of methyl acetate. The ethane formed undergoes subsequent reactions to form ethylene, as shown in reactions R6-R8. The large pool of methyl radicals present in the first few microseconds also reacts with

the ethylene present in the methyl acetate blend to form propene which undergoes subsequent reactions to form benzene, as shown in Figure 11. Due to this, more benzene is formed for the methyl acetate blend than the ethylene baseline mixture. The acetylene formation pathway is similar to that of the ethylene baseline case. The reduced amount of acetylene is due to the methyl acetate being converted to carbon dioxide and carbon monoxide.

Figure 16a shows some of the major pathways during oxidation of the 2-methylfuran blend at equivalence ratio of 8.6. Figure 16b compares simulated time-histories of important species formed for methylfuran blend and ethylene baseline mixture at 1800 K.

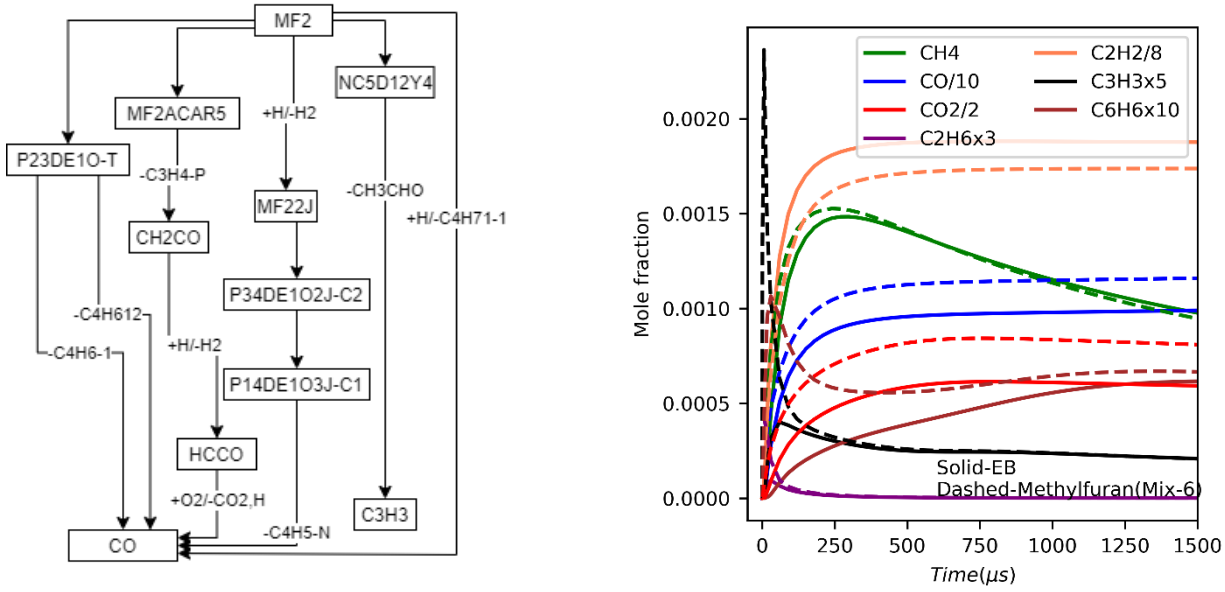

Figure 16. a) Major reaction pathways during oxidation of methylfuran-ethylene baseline mixture at 1800 K and equivalence ratio 8.6, b) Simulated time-histories of major species formed under this condition compared to the ethylene-baseline mixture.

At high temperature, 2-methyfuran undergoes ring-opening through reactions R30 and R31, and also rearranges via reaction R32. The products from R30 and R32 will eventually produce carbon monoxide and carbon dioxide, as shown in Figure 15(R33-R36). This increases in CO and CO_2 concentration in the methylfuran blend compared to the ethylene baseline mixture, as shown in Figure 16b. The increase in CO mole fraction is also evident in the experimental results shown in Figure 3.

MF2=P23DE1O-T	R30
MF2=NC5D12Y4	R31
MF2=MF2ACAR5	R32
P23DE1O-T=CO+C4H6-1	R33

P23DE1O-T=CO+C4H612	R34
MF2ACAR5=CH2CO+C3H4-P	R35
CH2CO+H=HCCO+H2	R36
HCCO+O2=CO+CO2+H	R37
NC5D12Y4=C3H3+CH3CO	R38

The NC5D12Y4 formed from reaction R31 readily decomposes to propargyl radical and acetaldehyde (R38). This is evident in the amount of propargyl formed from the 2-methyfuran blend in Figure 16b. The high amount of propargyl radical also increases the concentration of benzene in the mixture. Increased concentration of benzene and propargyl radical in methylfuran increases its sooting propensity compared to other oxygenated biofuels like ethanol and cyclopentanone[30].

The reaction pathway analysis shows significant differences in pathways for the formation of CO and C_2H_4 for these blends. Important soot precursors (e.g., acetylene and benzene) mole fractions differ drastically for most blends compared to the ethylene baseline mixture. Future works should include collecting high-quality data for species time-histories for these soot precursors.

5. Conclusions

High-temperature oxidation of Co-Optima biofuels blended with ethylene were conducted within the temperature range of 1700-2050 K at an equivalence ratio of 8.6. Carbon monoxide and ethylene time-histories were measured using laser absorption spectroscopy near 4.9 μm and 10.532 nm, respectively. Results reveal that oxygenated fuel blends produce more carbon monoxide than a diisobutylene-ethylene blend or ethylene baseline mixture within the temperature range in this work. In the oxygenated fuel blends, ethanol produced more CO than methyl acetate, followed by methylfuran. Ethanol also showed the fastest consumption of ethylene, while the diisobutylene blend showed the slowest consumption of ethylene. The results obtained were utilized to understand the performance of recent hydrocarbon and biofuel mechanisms from the literature. Most of the mechanisms were able to predict ethylene consumption at temperatures near 2000 K with high accuracy. At a lower temperature near 1700 K, several recent mechanisms over-predicted ethylene decay and CO formation time-histories. The Co-Optima mechanism was found to agree with experiment results throughout the temperature range of 1700-2050K. Pathway analysis was conducted using the Co-Optima mechanism, which revealed the important reactions involved in CO formation with different biofuel blends. The present work provides

the first high-temperature, time-resolved measurements of species during oxidation of these fuels at the fuel-rich conditions tested in a shock tube. The data will serve as a validation target for current and future chemical kinetic models of these fuels for use with computational fluid dynamic simulations.

6. Acknowledgments:

This material is based upon work supported by the U.S. Department of Energy's Office of Energy Efficiency and Renewable Energy (EERE) under Award Numbers DE-EE0007984 and DE-EE0007982 (Co-Optima). The work at LLNL was performed under the auspices of the U.S. Department of Energy (DOE), Contract DE-AC52-07NA27344 and was conducted as part of the Co-Optimization of Fuels & Engines (Co-Optima) project sponsored by the DOE Office of Energy Efficiency and Renewable Energy (EERE), Bioenergy Technologies and Vehicle Technologies Offices.

7. References

[1] Y. Yang, J.E. Dec, Bio-Ketones: Autoignition Characteristics and Their Potential as Fuels for HCCI Engines, SAE Int. J. Fuels Lubr. 6(3) (2013) 713-728.
[2] J.P. Szybist, S. Busch, R.L. McCormick, J.A. Pihl, D.A. Splitter, M.A. Ratcliff, C.P. Kolodziej, J.M.E. Storey, M. Moses-DeBusk, D. Vuilleumier, M. Sjöberg, C.S. Sluder, T. Rockstroh, P. Miles, What fuel properties enable higher thermal efficiency in spark-ignited engines?, Progress in Energy and Combustion Science 82 (2021) 100876.
[3] B. Rotavera, C.A. Taatjes, Influence of functional groups on low-temperature combustion chemistry of biofuels, Progress in Energy and Combustion Science, doi:https://doi.org/10.1016/j.pecs.2021.100925(2021) 100925.
[4] G. Barari, S.M. Sarathy, S.S. Vasu, Improved combustion kinetic model and HCCI engine simulations of di-isopropyl ketone ignition, Fuel 164 (2016) 141–150.

[5] R.L. McCormick, G. Fioroni, L. Fouts, E. Christensen, J. Yanowitz, E. Polikarpov, K. Albrecht, D.J. Gaspar, J. Gladden, A. George, Selection Criteria and Screening of Potential Biomass-Derived Streams as Fuel Blendstocks for Advanced Spark-Ignition Engines, SAE Int. J. Fuels Lubr. 10 (2017).
[6]

J. Farrell. Sponsor Org.: USDOE Office of Energy Efficiency and Renewable Energy (EERE), Bioenergy Technologies Office (EE-3B). Co-Optimization of Fuels and Engines. In: editor^editors. 2016-04-11 2016; United States. p.
[7] D.J. Gaspar, B.H. West, D. Ruddy, T.J. Wilke, E. Polikarpov, T.L. Alleman, A. George, E. Monroe, R.W. Davis, D. Vardon, A.D. Sutton, C.M. Moore, P.T. Benavides, J. Dunn, M.J. Biddy, S.B. Jones, M.D. Kass, J.A. Pihl, J.A. Pihl, M.M. Debusk, M. Sjoberg, J. Szybist, C.S. Sluder, G. Fioroni, W.J. Pitz, Top Ten Blendstocks Derived From Biomass For Turbocharged Spark Ignition Engines: Bio-blendstocks With Potential for Highest Engine Efficiency, United States, 2019-09-30, 2019.
[8] W.K. Metcalfe, W.J. Pitz, H.J. Curran, J.M. Simmie, C.K. Westbrook, The development of a detailed chemical kinetic mechanism for diisobutylene and comparison to shock tube ignition times, Proceedings of the Combustion Institute 31 (2007) 377-384.
[9] E. Hu, G. Yin, Z. Gao, Y. Liu, J. Ku, Z. Huang, Experimental and kinetic modeling study on 2,4,4-trimethyl-1-pentene ignition behind reflected shock waves, Fuel 195 (2017) 97-104.
[10] H. Li, Y. Qiu, Z. Wu, S. Wang, X. Lu, Z. Huang, Ignition delay of diisobutylene-containing multicomponent gasoline surrogates: Shock tube measurements and modeling study, Fuel 235 (2019) 1387-1399.
[11] S.M. Sarathy, P. Oßwald, N. Hansen, K. Kohse-Höinghaus, Alcohol combustion chemistry, Progress in Energy and Combustion Science 44 (2014) 40-102.
[12] C.-W. Wu, H. Matsui, N.-S. Wang, M.C. Lin, Shock Tube Study on the Thermal Decomposition of Ethanol, The Journal of Physical Chemistry A 115 (2011) 8086-8092.
[13]

Y. Hidaka, H. Wakamatsu, M. Moriyama, T. Koike, K. Yasunaga. Shock-tube study of ethanol pyrolysis. In: Z. Jiang, editor^editors. Shock Waves; 2005// 2005; Berlin, Heidelberg: Springer Berlin Heidelberg. p. 651-656.
[14] A.R. Laich, E. Ninnemann, S. Neupane, R. Rahman, S. Barak, W.J. Pitz, S.S. Goldsborough, S.S. Vasu, High-pressure shock tube study of ethanol oxidation: Ignition delay time and CO time-history measurements, Combustion and Flame 212 (2020) 486-499.
[15] M. Aghsaee, D. Nativel, M. Bozkurt, M. Fikri, N. Chaumeix, C. Schulz, Experimental study of the kinetics of ethanol pyrolysis and oxidation behind reflected shock waves and in laminar flames, Proceedings of the Combustion Institute 35 (2015) 393-400.
[16] J. Kiecherer, C. Bänsch, T. Bentz, M. Olzmann, Pyrolysis of ethanol: A shock-tube/TOF-MS and modeling study, Proceedings of the Combustion Institute 35 (2015) 465-472.
[17] L.T. Pinzón, O. Mathieu, C.R. Mulvihill, I. Schoegl, E.L. Petersen, Ethanol pyrolysis kinetics using H2O time history measurements behind reflected shock waves, Proceedings of the Combustion Institute 37 (2019) 239-247.
[18] K. Zhang, N. Lokachari, E. Ninnemann, S. Khanniche, W.H. Green, H.J. Curran, S.S. Vasu, W.J. Pitz, An experimental, theoretical, and modeling study of the ignition behavior of cyclopentanone, Proceedings of the Combustion Institute 37 (2019) 657-665.
[19] X. Dong, E. Ninnemann, D.S. Ranasinghe, A. Laich, R. Greene, S.S. Vasu, W.H. Green, Revealing the critical role of radical-involved pathways in high temperature cyclopentanone pyrolysis, Combustion and Flame 216 (2020) 280-292.

[20] S. Thion, C. Togbé, G. Dayma, Z. Serinyel, P. Dagaut, Experimental and Detailed Kinetic Modeling Study of Cyclopentanone Oxidation in a Jet-Stirred Reactor at 1 and 10 atm, Energy & Fuels 31 (2017) 2144-2155.
[21] A.P. Vyas, J.L. Verma, N. Subrahmanyam, A review on FAME production processes, Fuel 89 (2010) 1-9.
[22] A. Farooq, D.F. Davidson, R.K. Hanson, L.K. Huynh, A. Violi, An experimental and computational study of methyl ester decomposition pathways using shock tubes, Proceedings of the Combustion Institute 32 (2009) 247-253.
[23] W. Ren, K.-Y. Lam, D.F. Davidson, R.K. Hanson, X. Yang, Pyrolysis and oxidation of methyl acetate in a shock tube: A multi-species time-history study, Proceedings of the Combustion Institute 36 (2017) 255-264.
[24] A. Ahmed, W.J. Pitz, C. Cavallotti, M. Mehl, N. Lokachari, E.J.K. Nilsson, J.-Y. Wang, A.A. Konnov, S.W. Wagnon, B. Chen, Z. Wang, S. Kim, H.J. Curran, S.J. Klippenstein, W.L. Roberts, S.M. Sarathy, Small ester combustion chemistry: Computational kinetics and experimental study of methyl acetate and ethyl acetate, Proceedings of the Combustion Institute 37 (2019) 419-428.
[25] F.M.A. Geilen, T. vom Stein, B. Engendahl, S. Winterle, M.A. Liauw, J. Klankermayer, W. Leitner, Highly Selective Decarbonylation of 5-(Hydroxymethyl)furfural in the Presence of Compressed Carbon Dioxide, Angewandte Chemie International Edition 50 (2011) 6831-6834.
[26] K.P. Somers, J.M. Simmie, F. Gillespie, U. Burke, J. Connolly, W.K. Metcalfe, F. Battin-Leclerc, P. Dirrenberger, O. Herbinet, P.A. Glaude, H.J. Curran, A high temperature and atmospheric pressure experimental and detailed chemical kinetic modelling study of 2-methyl furan oxidation, Proceedings of the Combustion Institute 34 (2013) 225-232.
[27] Y. Uygun, S. Ishihara, H. Olivier, A high pressure ignition delay time study of 2-methylfuran and tetrahydrofuran in shock tubes, Combustion and Flame 161 (2014) 2519-2530.
[28] K.P. Somers, J.M. Simmie, F. Gillespie, C. Conroy, G. Black, W.K. Metcalfe, F. Battin-Leclerc, P. Dirrenberger, O. Herbinet, P.-A. Glaude, P. Dagaut, C. Togbé, K. Yasunaga, R.X. Fernandes, C. Lee, R. Tripathi, H.J. Curran, A comprehensive experimental and detailed chemical kinetic modelling study of 2,5-dimethylfuran pyrolysis and oxidation, combustion and flame 160 (2013) 2291-2318.
[29] L.-S. Tran, Z. Wang, H.-H. Carstensen, C. Hemken, F. Battin-Leclerc, K. Kohse-Höinghaus, Comparative experimental and modeling study of the low- to moderate-temperature oxidation chemistry of 2,5-dimethylfuran, 2-methylfuran, and furan, Combustion and Flame 181 (2017) 251-269.
[30] S. Barak, R.K. Rahman, S. Neupane, E. Ninnemann, F. Arafin, A. Laich, A.C. Terracciano, S.S. Vasu, Measuring the effectiveness of high-performance Co-Optima biofuels on suppressing soot formation at high temperature, Proceedings of the National Academy of Sciences 117 (2020) 3451.
[31] A.B. Dempsey, B.-L. Wang, R.D. Reitz, B. Petersen, D. Sahoo, P.C. Miles, Comparison of Quantitative In-Cylinder Equivalence Ratio Measurements with CFD Predictions for a Light Duty Low Temperature Combustion Diesel Engine, SAE International Journal of Engines 5 (2012) 162-184.
[32] B. Koroglu, O.M. Pryor, J. Lopez, L. Nash, S.S. Vasu, Shock tube ignition delay times and methane time-histories measurements during excess CO2 diluted oxy-methane combustion, Combustion and Flame 164 (2016) 152-163.
[33] S. Neupane, R.K. Rahman, J. Baker, F. Arafin, E. Ninnemann, K. Thurmond, C.-H. Wang, A.E. Masunov, S.S. Vasu, DMMP pyrolysis and oxidation studies at high temperature inside a shock tube using laser absorption measurements of CO, Combustion and Flame 214 (2020) 14-24.
[34] E. Ninnemann, O. Pryor, S. Barak, S. Neupane, Z. Loparo, A. Laich, S.S. Vasu, Reflected shock-initiated ignition probed via simultaneous lateral and endwall high-speed imaging with a transparent, cylindrical test-section, Combustion and Flame 224 (2021) 43-53.

[35] M.S. Johnson, M.R. Nimlos, E. Ninnemann, A. Laich, G.M. Fioroni, D. Kang, L. Bu, D. Ranasinghe, S. Khanniche, S.S. Goldsborough, S.S. Vasu, W.H. Green, Oxidation and pyrolysis of methyl propyl ether, International Journal of Chemical Kinetics 53 (2021) 915-938.
[36] K. Hakimov, F. Arafin, K. Aljohani, K. Djebbi, E. Ninnemann, S.S. Vasu, A. Farooq, Ignition delay time and speciation of dibutyl ether at high pressures, Combustion and Flame 223 (2021) 98-109.
[37] S. Dong, K. Zhang, E.M. Ninnemann, A. Najjar, G. Kukkadapu, J. Baker, F. Arafin, Z. Wang, W.J. Pitz, S.S. Vasu, S.M. Sarathy, P.K. Senecal, H.J. Curran, A comprehensive experimental and kinetic modeling study of 1- and 2-pentene, Combustion and Flame 223 (2021) 166-180.
[38] R.K. Rahman, S. Barak, K.R.V. Manikantachari, E. Ninnemann, A. Hosangadi, A. Zambon, S.S. Vasu, Probing the Effects of NOx and SOx Impurities on Oxy-Fuel Combustion in Supercritical CO2: Shock Tube Experiments and Chemical Kinetic Modeling, Journal of Energy Resources Technology 142 (2020).
[39] L.S. Rothman, I.E. Gordon, A. Barbe, D.C. Benner, P.F. Bernath, M. Birk, V. Boudon, L.R. Brown, A. Campargue, J.P. Champion, K. Chance, L.H. Coudert, V. Dana, V.M. Devi, S. Fally, J.M. Flaud, R.R. Gamache, A. Goldman, D. Jacquemart, I. Kleiner, N. Lacome, W.J. Lafferty, J.Y. Mandin, S.T. Massie, S.N. Mikhailenko, C.E. Miller, N. Moazzen-Ahmadi, O.V. Naumenko, A.V. Nikitin, J. Orphal, V.I. Perevalov, A. Perrin, A. Predoi-Cross, C.P. Rinsland, M. Rotger, M. Šimečková, M.A.H. Smith, K. Sung, S.A. Tashkun, J. Tennyson, R.A. Toth, A.C. Vandaele, J. Vander Auwera, The HITRAN 2008 molecular spectroscopic database, J. Quant. Spectrosc. Radiat. Transfer 110 (2009) 533-572.
[40] W. Ren, D.F. Davidson, R.K. Hanson, IR laser absorption diagnostic for C2H4 in shock tube kinetics studies, International Journal of Chemical Kinetics 44 (2012) 423-432.
[41] Z.E. Loparo, J.G. Lopez, S. Neupane, W.P. Partridge, K. Vodopyanov, S.S. Vasu, Fuel-rich n-heptane oxidation: A shock tube and laser absorption study, Combust. Flame 185 (2017) 220-233.
[42] C.-W. Zhou, Y. Li, U. Burke, C. Banyon, K.P. Somers, S. Ding, S. Khan, J.W. Hargis, T. Sikes, O. Mathieu, E.L. Petersen, M. AlAbbad, A. Farooq, Y. Pan, Y. Zhang, Z. Huang, J. Lopez, Z. Loparo, S.S. Vasu, H.J. Curran, An experimental and chemical kinetic modeling study of 1,3-butadiene combustion: Ignition delay time and laminar flame speed measurements, Combustion and Flame 197 (2018) 423-438.
[43] E. Ranzi, C. Cavallotti, A. Cuoci, A. Frassoldati, M. Pelucchi, T. Faravelli, New reaction classes in the kinetic modeling of low temperature oxidation of n-alkanes, Combustion and Flame 162 (2015) 1679-1691.
[44] H. Wang, E. Dames, B. Sirjean, D.A. Sheen, R. Tangko, A. Violi, J.Y.W. Lai, F.N. Egolfopoulos, D.F. Davidson, R.K. Hanson, A high-temperature chemical kinetic model of n-alkane (up to n-dodecane), cyclohexane, and methyl-, ethyl-, n-propyl and n-butyl-cyclohexane oxidation at high temperatures, JetSurF version 2 (2010) 19.
[45] A. Frassoldati, A. Cuoci, T. Faravelli, U. Niemann, E. Ranzi, R. Seiser, K. Seshadri, An experimental and kinetic modeling study of n-propanol and iso-propanol combustion, Combustion and Flame 157 (2010) 2-16.
[46] Z. Cheng, Y. Tan, L. Wei, L. Xing, J. Yang, L. Zhang, Y. Guan, B. Yan, G. Chen, D.Y.C. Leung, Experimental and kinetic modeling studies of furan pyrolysis: Fuel decomposition and aromatic ring formation, Fuel 206 (2017) 239-247.
[47] J. Shao, R. Choudhary, Y. Peng, D.F. Davidson, R.K. Hanson, Shock Tube Measurement of the C2H4 + H ⇔ C2H3 + H2 Rate Constant, J. Phys. Chem. A 123 (2019) 15-20.
[48] G.B. Skinner, R.C. Sweet, S.K. Davis, Shock tube experiments on the pyrolysis of deuterium-substituted ethylenes, The Journal of Physical Chemistry 75 (1971) 1-12.
[49] V.D. Knyazev, Á. Bencsura, S.I. Stoliarov, I.R. Slagle, Kinetics of the C2H3 + H2 ⇄ H + C2H4 and CH3 + H2 ⇄ H + CH4 Reactions, The Journal of Physical Chemistry 100 (1996) 11346-11354.
[50] W. Tsang, R.F. Hampson, Chemical Kinetic Data Base for Combustion Chemistry. Part I. Methane and Related Compounds, Journal of Physical and Chemical Reference Data 15 (1986) 1087-1279.

[51] S.L. Peukert, R. Sivaramakrishnan, M.-C. Su, J.V. Michael, Experiment and theory on methylformate and methylacetate kinetics at high temperatures: Rate constants for H-atom abstraction and thermal decomposition, Combustion and Flame 159 (2012) 2312-2323.